VOL. 23, NO. 2, 2024, 62-80
elektrika.utm.my
ISSN 0128-4428

ELEKTRIKA
Journal of Electrical Engineering

Identification of Multi-Microgrid Clusters Using Terminal Spectral Clustering Algorithm

Nurul Nadia Ibrahim, Jasrul Jamani Jamian* and Madihah Md Rasid

Faculty of Electrical Engineering, Universiti Teknologi Malaysia, 81310 UTM Skudai, Johor, Malaysia.

*Corresponding author: jasrul@utm.my

Abstract: In response to the increasing impact of extreme weather on power distribution networks (PDNs), prioritizing resilience is imperative. This study introduces an innovative k-means spectral clustering algorithm to define the boundaries of microgrids (MGs) within a multi-microgrid (MMG) system. The aim is to improve reliability by clustering PDNs into resilient MGs. The power systems are modeled with nodes representing buses, and connections are represented as edges. The analysis involves computing the adjacency matrix, degree matrix, Laplacian matrix, and applying k-means clustering to group buses based on terminal point features. Silhouette coefficients (SC) are calculated to assess the quality of the clustering. The proposed method is tested on three IEEE distribution systems: IEEE 33, 69, and 118 bus systems. Findings reveal distinct clusters within each system with SC values above 0.68, particularly emphasizing the significance of terminal points as the basis for assisting power engineers in decision-making for predetermined grid partitioning.

Keywords: multi-microgrid, Silhouette coefficients, spectral clustering algorithm, terminal points

© 2024 Penerbit UTM Press. All rights reserved

Article History: received 18 January 2024; accepted 9 May 2024; published 29 August 2024

1. INTRODUCTION

1.1 Motivation and Incitement

Weather events are a significant cause of power supply outages, as well as reliability and resiliency issues. In recent years, the global community has witnessed numerous extreme weather events, resulting in power outages, blackouts, and economic losses totaling billions of dollars. Hurricane Sandy in 2012 in the Eastern United States caused power outages for approximately 8,100,000 consumers. Likewise, the 2014 typhoon Rammasun in the Luzon region of the Philippines affected 13,000,000 customers, and the Blyth Tornado in 2016 impacted around 1,700,000 people in South Australia [1]. The February 2021 Texas outage demonstrated the profound impact a severe winter storm can have on a society, causing $195 billion in collateral damage and leaving nearly 4.5 million homes without electrical power [2].

Due to the increasing frequency and intensity of catastrophic events, ensuring the resilience of the power distribution networks (PDNs) has become a critical priority. About 90% of power outages caused by hurricanes occur in distribution networks. After catastrophic events, certain remote areas may experience power outages. Conventional load restoration techniques [3-6], which involve grid reconfiguration and require energization from the utility, may not ensure uninterrupted power supply following catastrophic events, potentially leading to prolonged outages for some users [7-8].

A microgrid (MG) consists of distributed energy resources (DERs) like solar panels, wind turbines, and interconnected loads that have distinct electrical boundaries. It is a locally regulated, independent system that is connected to the electrical grid. This is one method of protecting crucial loads (CLs). By enabling connections and disconnections from the grid, the MG allows operation in both grid-connected and islanded modes [9]. However, microgrids have the potential to operate beyond individual units, leading to the field of research known as multi-microgrids (MMGs). MMGs offer enhanced reliability, power quality, and flexibility for managing renewable energy sources (RESs). However, efficient implementation necessitates an innovative approach to their formation and management.

1.2 Clustering Power Distribution Network to Multiple Microgrids

Several methodologies have been proposed for clustering PDNs, as documented in Table 1. Studies referenced in [10-11], [12-13], and [14] identify the optimal ESD location, the optimal sectionalizing switch location, and the optimal power utilization as fundamental criteria for partitioning the distribution network.

Study [15] classifies the distribution system into partitions that can function as MGs using the k-means optimization method, determined by selecting the k-means with the maximum Silhouette score through the evaluation of the Silhouette approach. Additionally, [16] and [17] propose spectral clustering techniques that use dynamic weights of the lowest cost and line apparent power, respectively, to transform traditional systems into clusters of MMGs. The graph partitioning approach in [18] uses line susceptance as the weight during the clustering process.

References [19] and [20] utilize the count of generators to establish number of clusters, with [19] adopting the density-based spatial clustering of applications with noise

(DBSCAN) approach and [20] employing a mixed-integer linear programming (MILP) model as a different approach. In [21], the number of clusters is determined using constrained spectral clustering algorithm considering both the 'Must-Link' (ML) constraint and a minimum cut cost constraint. Meanwhile, the k-medoids spectral clustering algorithm used in [18] identifies suitable nodes for isolation but requires predefining the number of clusters. Reference [22] utilizes a hierarchical spectral clustering for determining clusters boundaries, allowing the adjustment of the number of clusters formed based on stakeholders' prior knowledge. However, this leaves the determination of the optimal number of clusters unspecified, lacking a specific criterion.

Despite extensive research into methods on establishing clusters within the distribution network, certain aspects of this process remain unaddressed in existing literature. Notably absent is a discussion on the predetermination of microgrid boundaries, especially concerning the optimal number of clusters (*k*) and their alignment with network topological characteristics. In contrast, this paper aims to bridge this gap by proposing an innovative approach for determining MG boundaries during the design phase. Utilizing the k-means clustering algorithm, our method introduces an innovative *k* selection technique based on total number of terminal points and Silhouette global coefficient. Additionally, the resulting cluster structure is improved through the incorporation of bi-layered filter approach.

Terminal points in a power grid are critical due to the potential of significant consequences resulting from disturbances at these points, which make them vulnerable as they are the farthest points with only one connection. Examining the clustering of terminal points assists in identifying network areas requiring special attention for resilience planning.

Unlike restoration and reconfiguration methods that address operations after an event, this study proposes pre-planning microgrid boundaries to optimize the utilization of DERs within those boundaries. This not only enhances energy efficiency and sustainability but also lays the groundwork for improved microgrid performance. Predefined microgrid boundaries enable efficient load distribution and minimize the need for extensive reconfiguration during outages, ultimately reducing grid congestion and facilitating faster response times.

Table 1. Comparison of the proposed method to other comparable works in the field of MMG partitioning

Ref.		13	16	11	18	19	17	20	21	22	Proposed approach
Year		2019	2019	2020	2022	2022	2023	2023	2023	2023	
MMG partitioning method	Optimum sectionalizing switch location	✓	-	-	-	-	-	-	-	-	-
	Improved spectral clustering	-	✓	-	-	-	-	-	-	-	-
	Optimum ESD location	-	-	✓	-	-	-	-	-	-	-
	Line susceptance with k-mediod spectral clustering	-	-	-	✓	-	-	-	-	-	-
	DBSCAN spatial clustering	-	-	-	-	✓	-	-		-	-
	Apparent power weighted graph partitioning approach	-	-	-	-	-	✓	-	-	-	-
	Constrained MILP	-	-	-	-	-	-	✓	-	-	-
	Constrained spectral clustering algorithm	-	-	-	-	-	-	-	✓	-	-
	Hierarchical spectral clustering	-	-	-	-	-	-	-	-	✓	-
	Terminal spectral clustering algorithm	-	-	-	-	-	-	-	-	-	✓
Type of weights	Static	-	-	-	✓	-	-	-	-	✓	✓
	Dynamic	-	✓	-	-	-	✓	-	✓	✓	-

2. FORMATION OF MICROGRIDS WITH BOUNDARIES

2.1 Terminal Spectral Clustering Algorithm

Spectral graph analysis has been employed to tackle challenges related to microgrids formation [23-28] and assess the stability of power networks [24]. The electricity grid can be intentionally clustered into smaller grids when there is an increasing risk of a cascade failure. Clustering the grid into separate, stable microgrids allows for the implementation of a complex procedure known as islanding, which helps mitigate the impact of cascading sequences on the electricity grid [28-30].

VOL. 23, NO. 2, 2024, 62-80
elektrika.utm.my
ISSN 0128-4428

ELEKTRIKA
Journal of Electrical Engineering

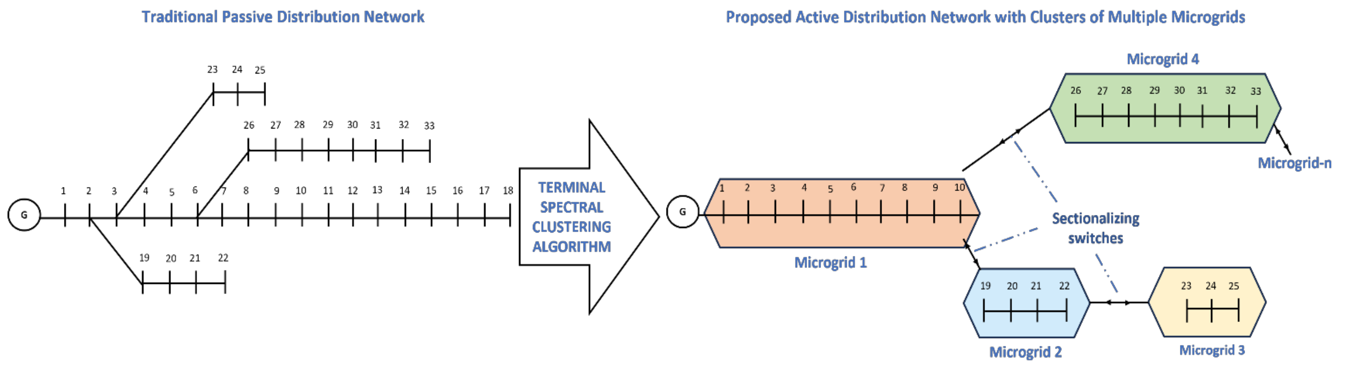

Figure 1. Proposed concept to partition existing distribution network to clusters of MMGs

This paper proposes a clustering approach [18] based on the terminal spectral clustering algorithm. The concept of the proposed methodology is presented in Figure 1. With this clustering method, the adjacency matrix (W) displays the connections between buses in a graph as binary relationships, as seen below:

$$W[i,j] = W[j,i] = \begin{cases} 1, & if\ bus\ i\ and\ j\ is\ connected \\ 0, & otherwise \end{cases} \quad (1)$$

In this case, if bus i is connected to bus j, the element *W[i,j]* represents the connection weight ij, or 0 if there is no direct connection. The weights of the existing connections between different buses are indicated by the non-null elements of the adjacency matrix, a $N \times N$ symmetric matrix.

The degree matrix *(D)* is a diagonal matrix in which the number of connections of bus i is represented by each diagonal element *D[i,j]*. It is formed based on the adjacency matrix, as shown in Equation (2).

$$D[i,j] = \sum W[i,:] \quad (2)$$

The distinction between the degree matrix and the adjacency matrix is explained in the definition of the Laplacian matrix *(L)* in Equation (3). The Laplacian matrix aids in understanding the local structure of the graph.

$$L = D - W \quad (3)$$

The connection described in Equation (4) can be determined by calculating the eigenvalues *(λ)* and eigenvectors *(v)* of the Laplacian matrix. The eigenvalues and associated eigenvectors produced by this process guide the spectral embedding procedure.

$$L \times v = \lambda \times v \quad (4)$$

In spectral embedding, the initial eigenvectors with the lowest eigenvalues are selected. By using these eigenvectors, a new matrix X is created, in which a bus is represented by each row and a feature generated from the eigenvectors is represented by each column.

The spectral embedding matrix X undergoes k-means clustering to group buses into clusters. The cluster number *(k)* was determined by considering the properties of the terminal points; the total number of buses with only one connection forms the basis for the clustering process. Figure 2 illustrates the overall proposed MMG clustering process.

2.2 Clustering Evaluation

To validate the clustering outcome, the Silhouette Coefficient (SC) [15] is utilized as a quality assessment metric. The formula for SC for a single data point is as follows:

$$s(i) = \frac{b(i) - a(i)}{max\{a(i), b(i)\}} \quad (5)$$

where *s(i)* is the SC for data point *i*, *a(i)* is the average distance from the *i-th* data point to other data points in the same cluster (cohesion), and *b(i)* is the smallest average distance from the *i-th* data point to data points in a different cluster (separation).

Equation (6) represents the average silhouette score for cluster *c*, while equation (7) formulates the overall average silhouette score for the entire set of data points.

$$AvgSC(c) = \frac{\sum s(i)}{number\ of\ i\ in\ cluster\ c} \quad (6)$$

$$OverallAvgSC = \frac{\sum s(i)}{total\ number\ of\ i} \quad (7)$$

The interpretations of the interval coefficient, as shown in Table 2, can be used to evaluate the results of SC interpretation.

Table 2. Interpretation of silhouette coefficient

Type	Interval silhouette coefficient	Interpretation
1	0.71 – 1.0	Robust structure

2	0.51 – 0.70	Satisfactory structure
3	0.26 – 0.50	Weak structure
4	< 0.25	No significant structure discovered

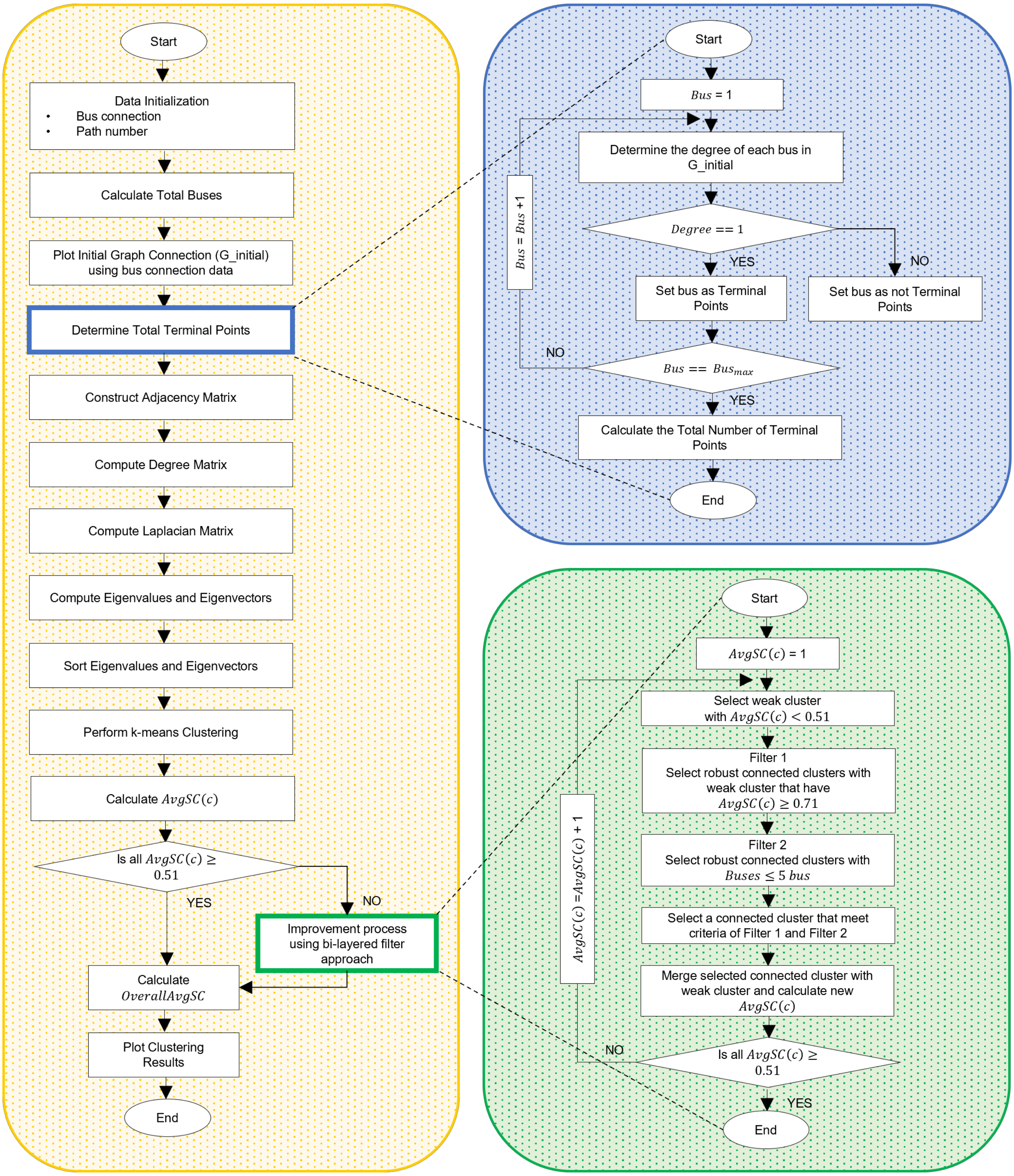

Figure 2. Terminal spectral clustering algorithm process

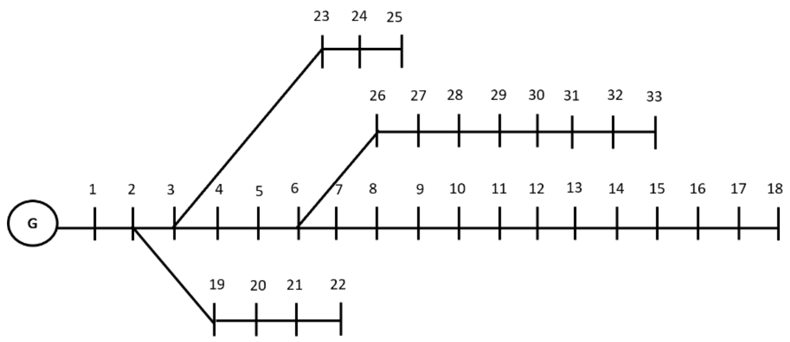

Figure 3. IEEE 33-bus test system

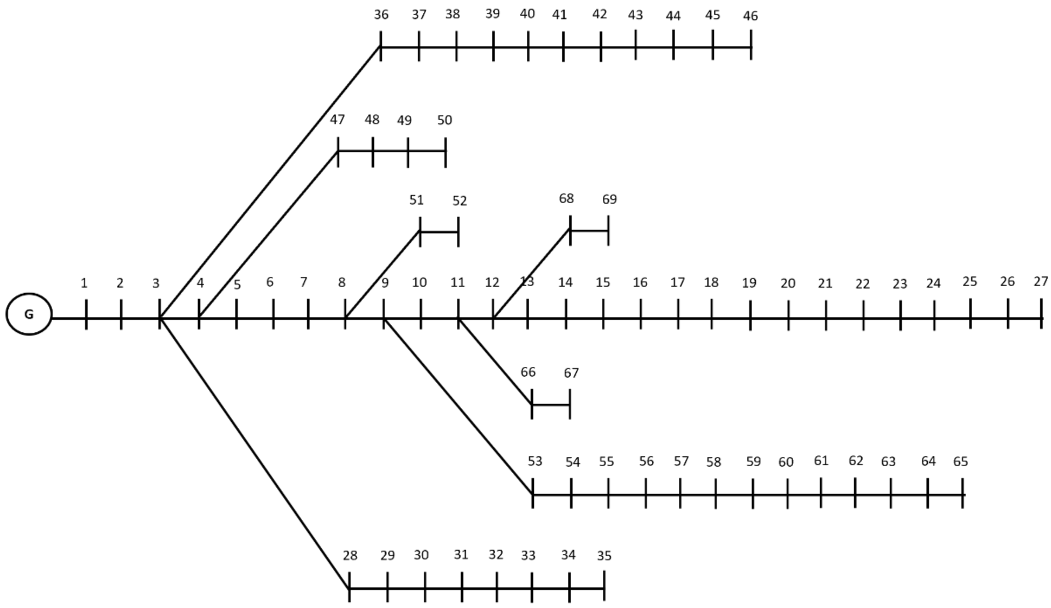

Figure 4. IEEE 69-bus test system

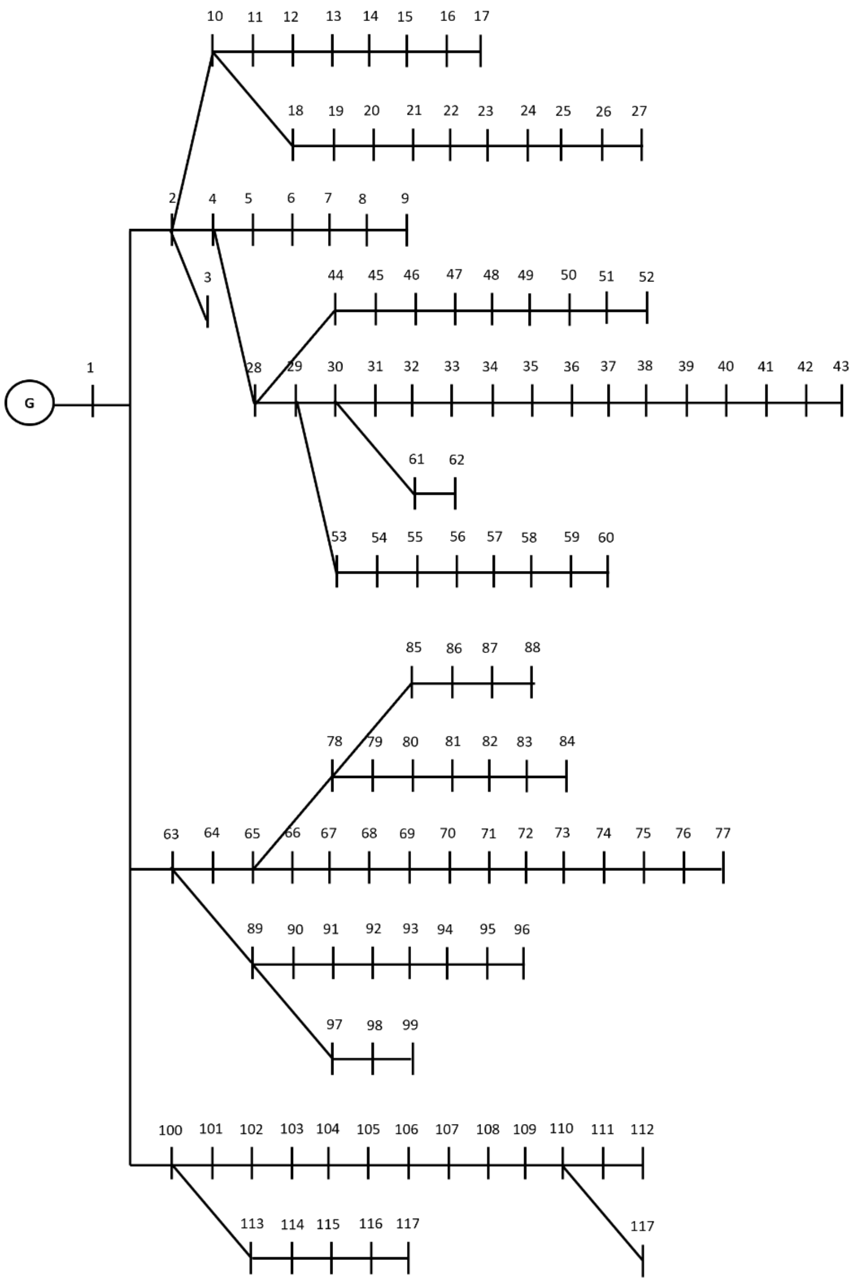

Figure 5. IEEE 118-bus test system

3. CASE STUDY

Three test systems [31-34] were used to evaluate the performance of the proposed algorithm. The line and bus data for the three test systems can be found in Appendices A to F. Test systems with different sizes were chosen to verify the computational efficiency of the proposed algorithm and its applicability to standard grid systems. Figures 3 to 5 show the initial conditions of the test systems.

4. RESULTS AND DISCUSSIONS

This section evaluates the efficacy of the proposed method by applying it to the IEEE 33-bus, IEEE 69-bus, and IEEE 118-bus test systems. MATLAB is utilized to simulate the clustering process. As outlined subsequently, a new k-means spectral clustering technique is tested on each of the mentioned systems, resulting in a clustering solution.

4.1 IEEE 33 bus test case

The effectiveness of the proposed methodology is demonstrated through its application to the IEEE 33 bus system, where the spectral clustering algorithm efficiently determines the partitioning based on identified terminal point numbers. As shown in Figure 6, buses 1, 18, 22, 25, and 33 are identified as terminal points, distinguished by their degree value of one. Consequently, this yields a comprehensive clustering outcome, indicating a total of five distinct clusters within the IEEE 33 bus system.

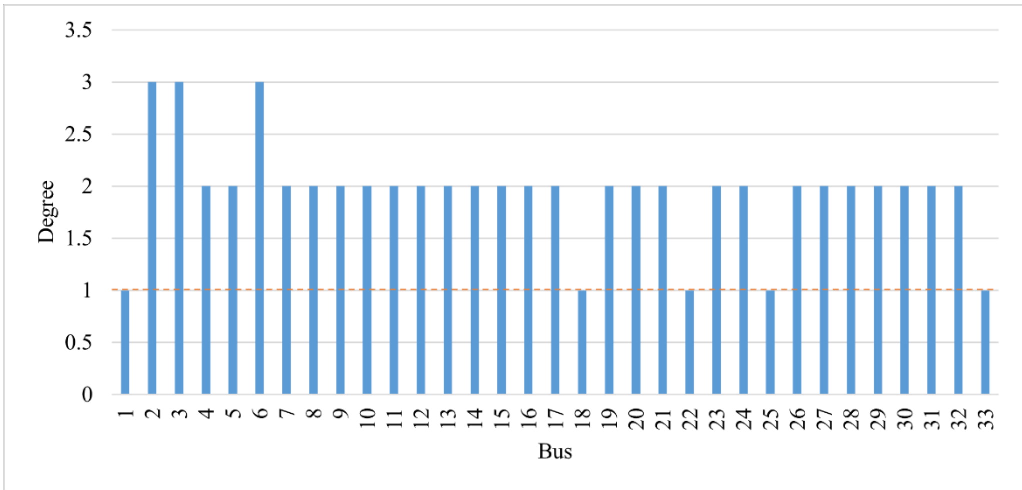

Figure 6. Degree matrix of IEEE 33 bus system

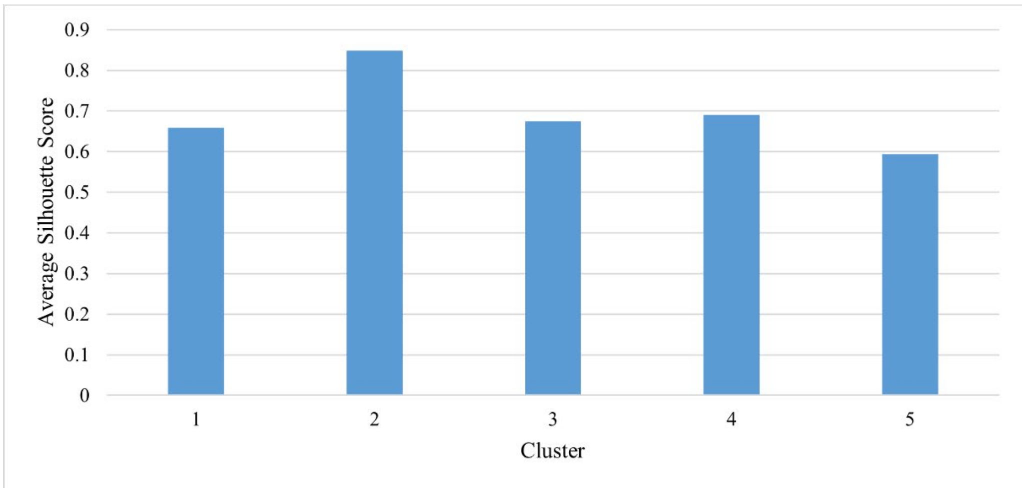

Figure 7. Average Silhouette score per cluster for IEEE 33 bus system

Figure 7 illustrates the average Silhouette score for each cluster, serving as a quantitative metric of clustering efficacy. Cluster 2 stands out with the highest score of 0.8481, indicating a well-defined and internally cohesive structure. Cluster 5 has the lowest score of 0.5934, suggesting a lower level of intra-cluster cohesion. The overall average Silhouette score of 0.68911 confirms the presence of a satisfactory clustering pattern.

Notably, the cluster with the highest Silhouette score shows a compact structure with minimal inter-node distances, emphasizing the cohesiveness within. Conversely, the cluster with the lowest score, particularly around bus 2, reveals a more branched and potentially disparate arrangement.

To facilitate the practical implementation of the proposed MMG partitioning strategy, detailed information on the composition of each cluster is provided in Tables 3 and 4. These tables offer a comprehensive breakdown, with Table 3 detailing the specific buses within each cluster and Table 4 focusing on the locations of sectionalizing switches. Additionally, Figure 8 visually presents the modified IEEE 33 bus system, illustrating the identified clusters with total load of each cluster.

Table 3. Network partitioning results for each cluster of the IEEE 33 bus test system

Clusters	Bus index
Microgrid 1	5, 6, 7, 8, 9, 10, 11, 12, 26, 27
Microgrid 2	28, 29, 30, 31, 32, 33
Microgrid 3	13, 14, 15, 16, 17, 18
Microgrid 4	3, 4, 23, 24, 25
Microgrid 5	1, 2, 19, 20, 21, 22

Table 4. Sectionalizing switch location of the IEEE 33 bus test system

Clusters	Location
Microgrid 1	Line 4-5, 12-13
Microgrid 2	Line 27-28
Microgrid 3	Line 12-13
Microgrid 4	Line 2-3, 4-5
Microgrid 5	Line 2-3

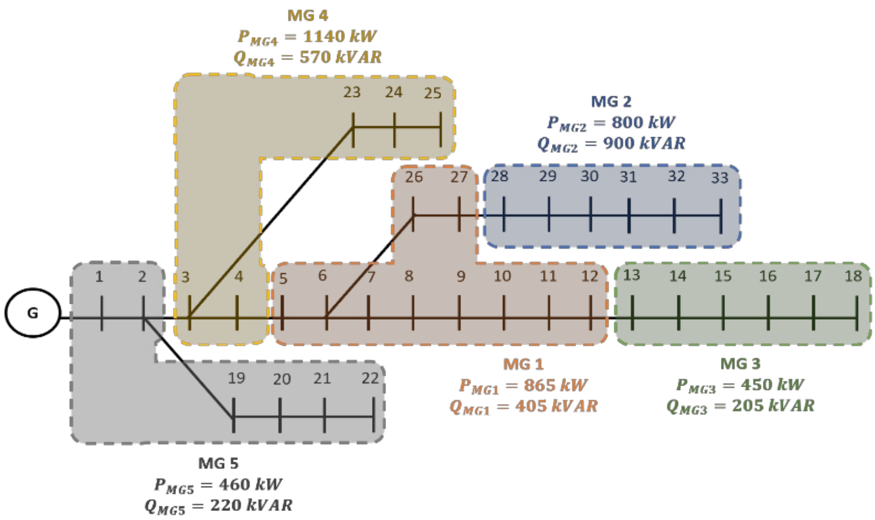

Figure 8. Proposed MMG formation of IEEE 33 bus test system

4.2 IEEE 69 bus test case

In the second test case with the IEEE 69 bus system, Figure 9 demonstrates that buses 1, 27, 35, 46, 50, 52, 65, 67, and 69 serve as terminal points resulting in a total of nine distinct clusters.

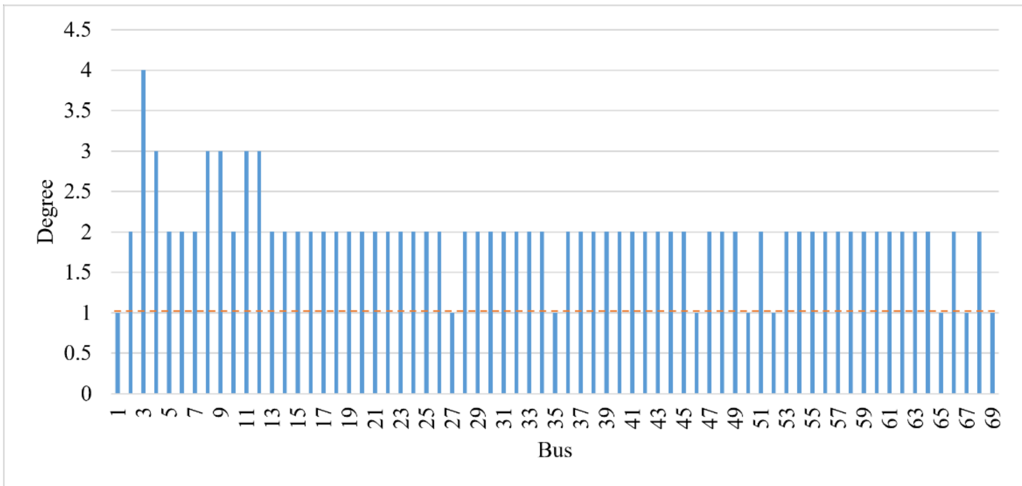

Figure 9. Degree matrix of IEEE 69 bus system

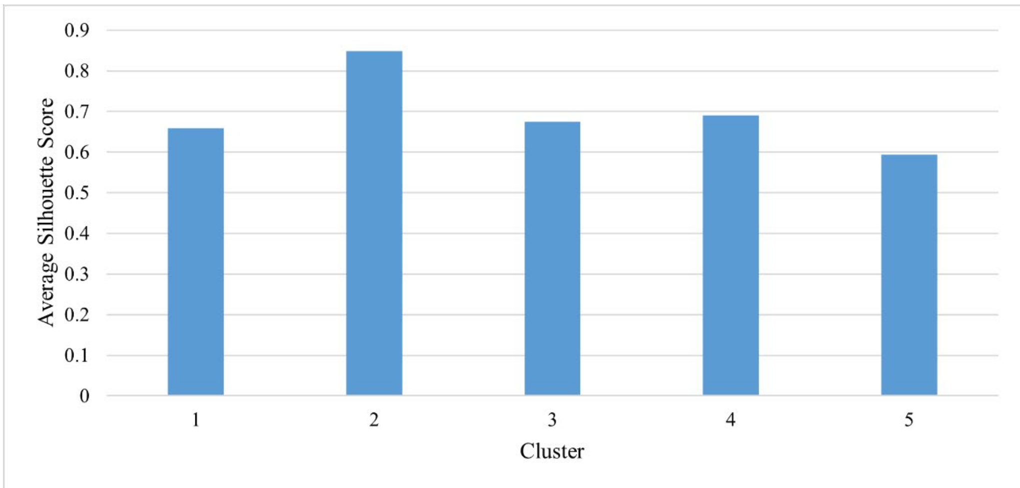

Figure 10. Average Silhouette score per cluster for IEEE 69 bus system

Figure 10 illustrates the average Silhouette score for each cluster, providing a quantitative measure of how effectively the clusters are formed. Cluster 7 stands out with the highest score of 0.8490, signifying a well-defined and internally cohesive structure. In contrast, Cluster 3, with the lowest score of 0.5904, indicates a lower level of intra-cluster cohesion. The overall average Silhouette score of 0.69507 confirms the existence of a recognizable clustering pattern. The composition of each cluster is further elaborated on in Tables 5 and 6. Table 5 details bus locations, while Table 6 pinpoints the placement of sectionalizing switches within each cluster. Examining Table 5 and Figure 11, it is evident that the cluster with the lowest score exhibits a greater number of buses, while the cluster with the highest score displays a smaller number of buses.

Table 5. Network partitioning results for each cluster of the IEEE 69 bus test system

Clusters	Bus index
Microgrid 1	41, 42, 43, 44, 45, 46
Microgrid 2	14, 15, 16, 17, 18, 19, 20, 21
Microgrid 3	7, 8, 9, 51, 52, 53, 54, 55, 56, 57, 58, 59
Microgrid 4	1, 2, 3, 4, 28, 29, 5, 6, 36, 37, 38, 39, 40
Microgrid 5	30, 31, 32, 33, 34, 35
Microgrid 6	60, 61, 62, 63, 64, 65
Microgrid 7	10, 11, 12, 13, 66, 67, 68, 69
Microgrid 8	47, 48, 49, 50
Microgrid 9	22, 23, 24, 25, 26, 27

Table 6. Sectionalizing switch location of the IEEE 69 bus test system

Clusters	Location
Microgrid 1	Line 40-41
Microgrid 2	Line 13-14, 21-22
Microgrid 3	Line 6-7, 9-10, 59-60
Microgrid 4	Line 6-7, 29-30, 40-41
Microgrid 5	Line 29-30
Microgrid 6	Line 59-60
Microgrid 7	Line 9-10, 13-14
Microgrid 8	Line 4-47
Microgrid 9	Line 21-22

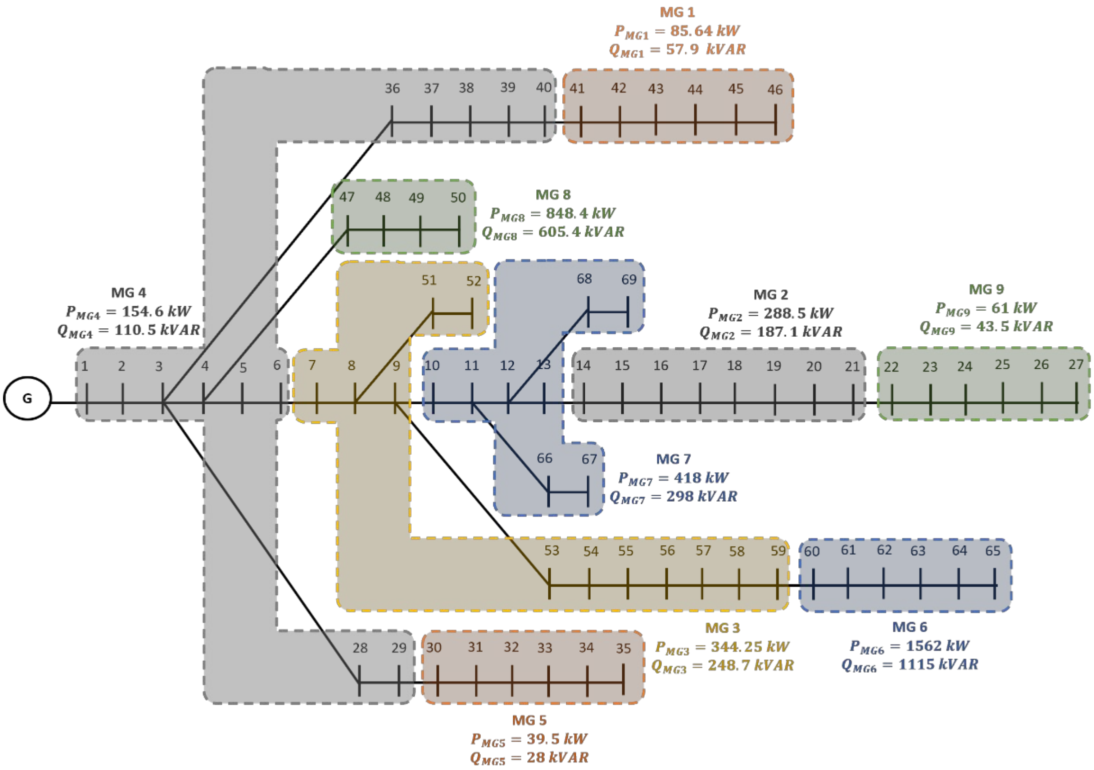

Figure 11. Proposed MMG formation of IEEE 69 bus test system

4.3 IEEE 118 bus test case

Buses 3, 9, 17, 27, 43, 52, 60, 62, 77, 84, 88, 96, 99, 112, 117, and 118 are recognised as terminal points in the third test scenario, which involves the IEEE 118 bus system. Each of these buses is represented by a degree value of one in Figure 12. As a result, the IEEE 118 bus system is proposed to have 16 different clusters.

Figure 13 shows that Cluster 10 has the highest score of 0.8694, suggesting a well-defined and internally consistent structure. Cluster 3, however, has the lowest intra-cluster cohesion score of 0.3547, indicating a weak structure that falls below the desired threshold of 0.51 as interpreted in Table 2.

To improve the cluster structure and ensure all clusters have a score above 0.50, a bi-layered filter approach is introduced (see Figure 2). The first filter selects the robust clusters (SC above 0.7) that connected to weak clusters (SC below 0.51). In the second filter, only connected clusters with a bus count less than or equal to 5 are considered. The connected cluster fulfilling both criteria (high SC and low bus count) is then selected for merging with the weak cluster. In this case, cluster 7 with an SC of 0.8614 and 5 buses is chosen for merging with cluster 3. The merged cluster has a resulting SC value of 0.5439.

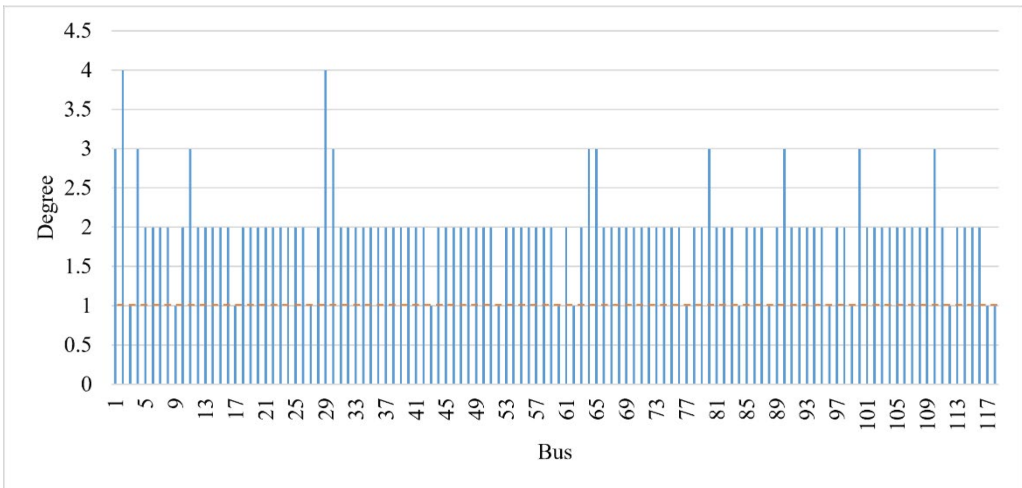

Figure 12. Degree matrix of 118 bus system

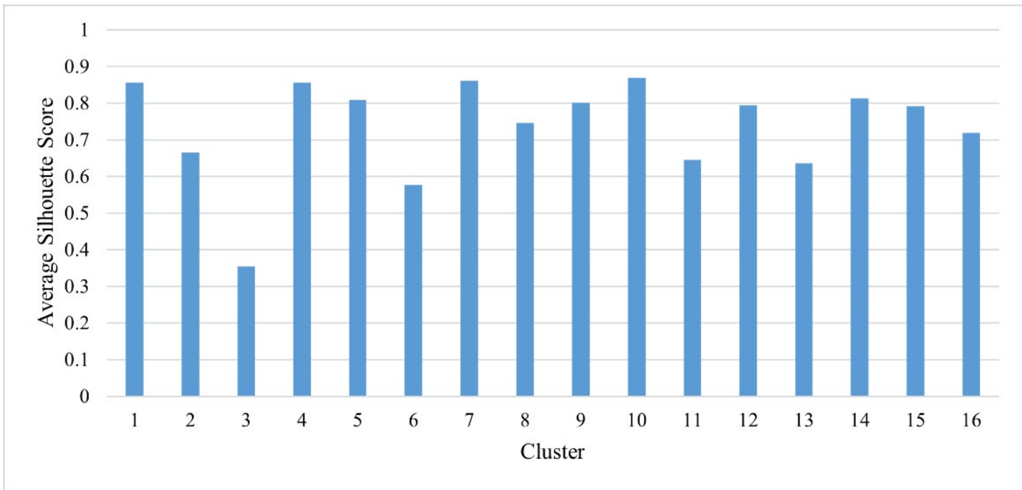

Figure 13. Average Silhouette score per cluster for IEEE 118 bus system

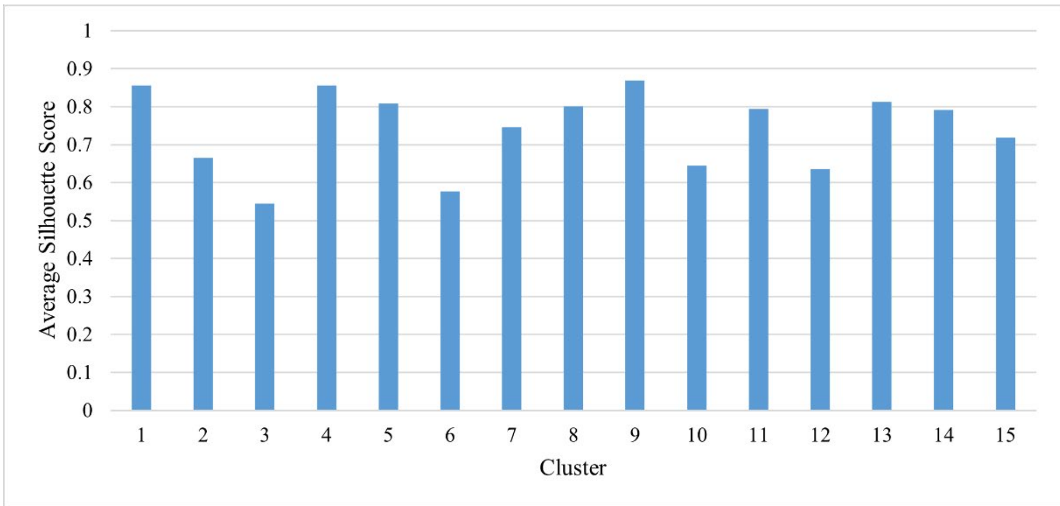

Figure 14. Improved average Silhouette score per cluster for IEEE 118 bus system

Figure 14 shows that the average Silhouette score for the IEEE 118 bus system is now above 0.51 for all clusters, indicating a satisfactory structure after the improvement process. The resulting clustering pattern with 15 clusters has an overall average Silhouette score of 0.69339.

Table 7. Network partitioning results for each cluster of the IEEE 118 bus test system

Clusters	Bus index
Microgrid 1	38, 39, 40, 41, 42, 43
Microgrid 2	89, 90, 91, 97, 98, 99
Microgrid 3	1, 2, 3, 4, 5, 6, 7, 8, 9, 10, 11, 12, 13, 14, 15, 16, 17, 18, 19, 63
Microgrid 4	85, 86, 87, 88
Microgrid 5	92, 93, 94, 95, 96
Microgrid 6	64, 65, 66, 67, 68, 69, 70, 71, 72, 78, 79
Microgrid 7	45, 46, 47, 48, 49, 50, 51, 52
Microgrid 8	73, 74, 75, 76, 77
Microgrid 9	20, 21, 22, 23, 24, 25, 26, 27
Microgrid 10	28, 29, 30, 31, 32, 33, 34, 35, 36, 37, 44, 53, 61, 62
Microgrid 11	108, 109, 110, 111, 112, 118
Microgrid 12	80, 81, 82, 83, 84
Microgrid 13	113, 114, 115, 116, 117

Microgrid 14	54, 55, 56, 57, 58, 59, 60
Microgrid 15	100, 101, 102, 103, 104, 105, 106, 107

Table 8. Sectionalizing switch location of the IEEE 118 bus test system

Clusters	Location
Microgrid 1	Line 37-38
Microgrid 2	Line 63-89, 91-92
Microgrid 3	Line 4-28, 19-20, 63-64, 1-100
Microgrid 4	Line 78-85
Microgrid 5	Line 91-92
Microgrid 6	Line 63-64, 72-73, 78-85, 80-81
Microgrid 7	Line 44-45
Microgrid 8	Line 72-73
Microgrid 9	Line 19-20
Microgrid 10	Line 4-28, 37-38, 44-45, 53-54
Microgrid 11	Line 107-108
Microgrid 12	Line 79-80
Microgrid 13	Line 100-113
Microgrid 14	Line 53-54
Microgrid 15	Line 1-100, 107-108

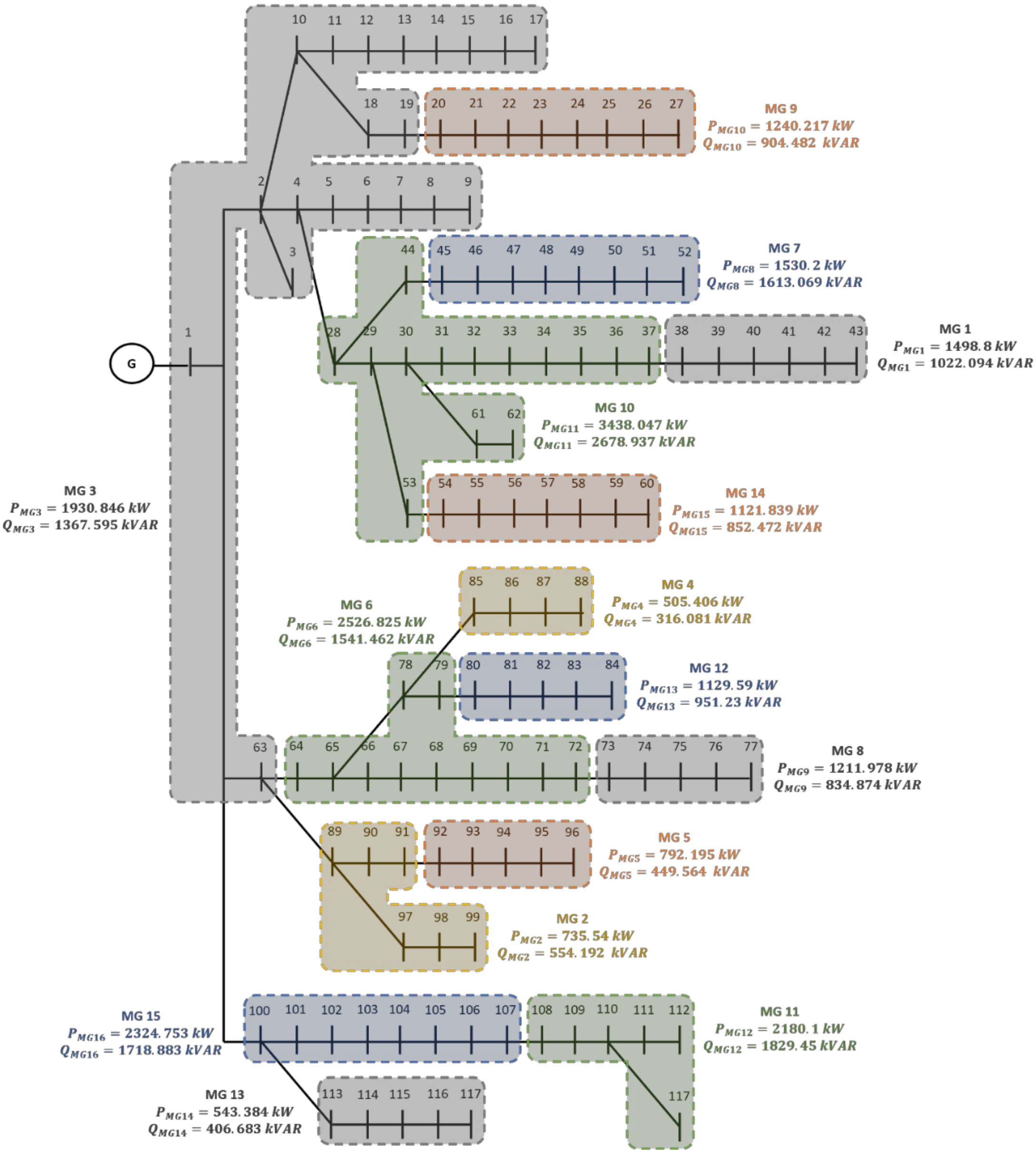

Figure 15. Proposed MMG formation of IEEE 118 bus test system

Supporting the practical application of this MMG partitioning strategy, Tables 7 and 8 provide a detailed breakdown of each cluster's composition. Specifically, Table 7 details the buses belonging to each cluster, and Table 8 focuses on the locations of sectionalizing switches. As seen in Figure 15, the cluster with the lowest score has six branches, whereas the cluster with the greatest score has only one branch.

Table 9 summarizes the required time to execute the proposed method using MATLAB R2020a for each of the test systems. The simulation is performed using a laptop equipped with Windows 11, AMD Ryzen 5 5600H 3.30 GHz processor and 16 GB RAM.

Table 9. Computational time required for the proposed methodology

Category	Power system	Time (s)
Small	IEEE 33-bus test system	0.045
Medium	IEEE 69-bus test system	0.052
Large	IEEE 118-bus test system	0.111

5. CONCLUSION

This paper presents an innovative approach to improve the resilience of PDNs in the face of increasing challenges caused by extreme weather events. The approach involves establishing the boundaries of MGs in MMG system by utilising k-means spectral clustering algorithm. This technique efficiently groups buses based on terminal point features, whereas the problem formulation involves an extensive modeling of power systems, incorporating nodes and connections through adjacency matrices, degree matrices, and Laplacian matrices.

Assessments of the clustering results are performed using Silhouette coefficients. The findings obtained from evaluating the proposed method on IEEE 33, 69, and 118 bus systems demonstrate the presence of distinct clusters within each system, with overall average Silhouette score consistently exceeding 0.68. The visualisation of clustering results emphasises the efficacy of the method, demonstrating strong physical connections between buses inside each cluster and the absence of isolated buses without any physical connections. The importance of terminal points as a basic element for decision-making in grid partitioning has been demonstrated by these findings.

By prioritising terminal points in clustering, the findings of this paper can assist decision-makers and power engineers in optimising grid partitioning thereby improving the resilience of PDNs. Overall, this finding holds significant potential in minimising the impact of severe infrastructure disruptions in PDNs caused by extreme weather events.

While this work establishes the groundwork for MMG formation by defining MG boundaries, future studies will explore incorporating DERs and islanding constraints for a more practical implementation. This may involve optimizing DER sizing and developing operational strategies for MMG in both grid-connected and islanded states.

REFERENCES

[1] F. H. Jufri, V. Widiputra, and J. Jung, “State-of-the-art review on power grid resilience to extreme weather events: Definitions, frameworks, quantitative assessment methodologies, and enhancement strategies,” Applied Energy, vol. 239, pp. 1049–1065, Apr. 2019, doi: 10.1016/j.apenergy.2019.02.017.

[2] I. Diahovchenko, G. Kandaperumal, and A. Srivastava, “Enabling Resiliency Using Microgrids with Dynamic Boundaries,” SSRN Electronic Journal, 2022, Published, doi: 10.2139/ssrn.4074486.

[3] H. R. Esmaeilian and R. Fadaeinedjad, “Energy Loss Minimization in Distribution Systems Utilizing an Enhanced Reconfiguration Method Integrating Distributed Generation,” IEEE Systems Journal, vol. 9, no. 4, pp. 1430–1439, Dec. 2015, doi: 10.1109/jsyst.2014.2341579.

[4] M. W. Siti, D. V. Nicolae, A. A. Jimoh, and A. Ukil, “Reconfiguration and Load Balancing in the LV and MV Distribution Networks for Optimal Performance,” IEEE Transactions on Power Delivery, vol. 22, no. 4, pp. 2534–2540, Oct. 2007, doi: 10.1109/tpwrd.2007.905581.

[5] C. Lee, C. Liu, S. Mehrotra, and Z. Bie, “Robust Distribution Network Reconfiguration,” IEEE Transactions on Smart Grid, vol. 6, no. 2, pp. 836–842, Mar. 2015, doi: 10.1109/tsg.2014.2375160.

[6] X. Chen, W. Wu, and B. Zhang, “Robust Restoration Method for Active Distribution Networks,” IEEE Transactions on Power Systems, vol. 31, no. 5, pp. 4005–4015, Sep. 2016, doi: 10.1109/tpwrs.2015.2503426.

[7] T. Ding, Y. Lin, Z. Bie, and C. Chen, “A resilient microgrid formation strategy for load restoration considering master-slave distributed generators and topology reconfiguration,” Applied Energy, vol. 199, pp. 205–216, Aug. 2017, doi: 10.1016/j.apenergy.2017.05.012.

[8] C. Chen, J. Wang, F. Qiu, and D. Zhao, “Resilient Distribution System by Microgrids Formation After Natural Disasters,” IEEE Transactions on Smart Grid, vol. 7, no. 2, pp. 958–966, Mar. 2016, doi: 10.1109/tsg.2015.2429653.

[9] DOE, Summary report: 2012 DOE Microgrid Workshop, U.S. Dep. Energy, 2012, pp. 1–33

[10] H. Haddadian and R. Noroozian, “Multi-microgrids approach for design and operation of future distribution networks based on novel technical indices,” Applied Energy, vol. 185, pp. 650–663, Jan. 2017, doi: 10.1016/j.apenergy.2016.10.120.

[11] F. Moghateli, S. A. Taher, A. Karimi, and M. Shahidehpour, “Multi-objective design method for construction of multi-microgrid systems in active distribution networks,” IET Smart Grid, vol. 3, no. 3, pp. 331–341, Apr. 2020, doi: 10.1049/iet-stg.2019.0171.

[12] F. S. Gazijahani and J. Salehi, “Robust Design of Microgrids With Reconfigurable Topology Under Severe Uncertainty,” IEEE Transactions on Sustainable Energy, vol. 9, no. 2, pp. 559–569, Apr. 2018, doi: 10.1109/tste.2017.2748882.

[13] T. Khalili, M. T. Hagh, S. G. Zadeh, and S. Maleki, “Optimal reliable and resilient construction of dynamic self-adequate multi-microgrids under large-scale events,” IET Renewable Power Generation, vol. 13, no. 10, pp. 1750–1760, May 2019, doi: 10.1049/iet-rpg.2018.6222.

[14] S. A. Arefifar, M. Ordonez, and Y. A.-R. I. Mohamed, “Voltage and Current Controllability in Multi-Microgrid Smart Distribution Systems,” IEEE Transactions on Smart Grid, vol. 9, no. 2, pp. 817–826, Mar. 2018, doi: 10.1109/tsg.2016.2568999.

[15] S. Hasanvand, M. Nayeripour, S. A. Arefifar, and H. Fallahzadeh-Abarghouei, “Spectral clustering for designing robust and reliable multi-MG smart distribution systems,” IET Generation, Transmission & Distribution, vol. 12, no. 6, pp. 1359–1365, Feb. 2018, doi: 10.1049/iet-gtd.2017.0671.

[16] M. Goubko and V. Ginz, “Improved spectral clustering for multi-objective controlled islanding of power grid,” Energy Systems, vol. 10, no. 1, pp. 59–94, May 2017, doi: 10.1007/s12667-017-0240-1.

[17] R. Sireesha, C. Srinivasa Rao, and M. Vijay Kumar, “Graph theory based transformation of existing Distribution network into clusters of multiple micro-grids for reliability enhancement,” Materials Today: Proceedings, vol. 80, pp. 2921–2928, 2023, doi: 10.1016/j.matpr.2021.07.067.

[18] R. Rocchetta, “Enhancing the resilience of critical infrastructures: Statistical analysis of power grid spectral clustering and post-contingency vulnerability metrics,” Renewable and Sustainable Energy Reviews, vol. 159, p. 112185, May 2022, doi: 10.1016/j.rser.2022.112185.

[19] S. F. Mahdavizadeh, M. R. Aghamohammadi, and S. Ranjbar, “Frequency stability-based controlled islanding scheme based on clustering algorithm and electrical distance using real-time dynamic criteria

from WAMS data," Sustainable Energy, Grids and Networks, vol. 30, p. 100560, Jun. 2022, doi: 10.1016/j.segan.2021.100560.

[20] A. Amini Badr, A. Safari, and S. Najafi Ravadanegh, "Segmentation of interconnected power systems considering microgrids and the uncertainty of renewable energy sources," IET Generation, Transmission & Distribution, vol. 17, no. 17, pp. 3814–3827, Jul. 2023, doi: 10.1049/gtd2.12934.

[21] M. Salama, W. El-Dakhakhni, and M. Tait, "Systemic risk mitigation strategy for power grid cascade failures using constrained spectral clustering," International Journal of Critical Infrastructure Protection, vol. 42, p. 100622, Sep. 2023, doi: 10.1016/j.ijcip.2023.100622.

[22] J. Wu, X. Chen, S. Badakhshan, J. Zhang, and P. Wang, "Spectral Graph Clustering for Intentional Islanding Operations in Resilient Hybrid Energy Systems," IEEE Transactions on Industrial Informatics, vol. 19, no. 4, pp. 5956–5964, Apr. 2023, doi: 10.1109/tii.2022.3199240.

[23] R. J. Sanchez-Garcia et al., "Hierarchical Spectral Clustering of Power Grids," IEEE Transactions on Power Systems, vol. 29, no. 5, pp. 2229–2237, Sep. 2014, doi: 10.1109/tpwrs.2014.2306756.

[24] Y. Koç, M. Warnier, P. Van Mieghem, R. E. Kooij, and F. M. T. Brazier, "A topological investigation of phase transitions of cascading failures in power grids," Physica A: Statistical Mechanics and its Applications, vol. 415, pp. 273–284, Dec. 2014, doi: 10.1016/j.physa.2014.07.083.

[25] A. E. David and G. Sansavini, "Identification of critical states in power systems by limit state surface reconstruction," International Journal of Electrical Power & Energy Systems, vol. 101, pp. 162–175, Oct. 2018, doi: 10.1016/j.ijepes.2018.03.004.

[26] R. Mena, M. Hennebel, Y.-F. Li, C. Ruiz, and E. Zio, "A risk-based simulation and multi-objective optimization framework for the integration of distributed renewable generation and storage," Renewable and Sustainable Energy Reviews, vol. 37, pp. 778–793, Sep. 2014, doi: 10.1016/j.rser.2014.05.046.

[27] A. Abedi, L. Gaudard, and F. Romerio, "Power flow-based approaches to assess vulnerability, reliability, and contingency of the power systems: The benefits and limitations," Reliability Engineering & System Safety, vol. 201, p. 106961, Sep. 2020, doi: 10.1016/j.ress.2020.106961.

[28] Y.-P. Fang and E. Zio, "Unsupervised spectral clustering for hierarchical modelling and criticality analysis of complex networks," Reliability Engineering & System Safety, vol. 116, pp. 64–74, Aug. 2013, doi: 10.1016/j.ress.2013.02.021.

[29] M. Golari, N. Fan, and J. Wang, "Two-stage stochastic optimal islanding operations under severe multiple contingencies in power grids," Electric Power Systems Research, vol. 114, pp. 68–77, Sep. 2014, doi: 10.1016/j.epsr.2014.04.007.

[30] E. Ferrario, N. Pedroni, and E. Zio, "Evaluation of the robustness of critical infrastructures by Hierarchical Graph representation, clustering and Monte Carlo simulation," Reliability Engineering & System Safety, vol. 155, pp. 78–96, Nov. 2016, doi: 10.1016/j.ress.2016.06.007.

[31] V. Vita, "Development of a Decision-Making Algorithm for the Optimum Size and Placement of Distributed Generation Units in Distribution Networks," Energies, vol. 10, no. 9, p. 1433, Sep. 2017, doi: 10.3390/en10091433.

[32] A. F. Abdul Kadir, A. Mohamed, H. Shareef, and M. Z. Che Wanik, "Optimal placement and sizing of distributed generations in distribution systems for minimizing losses and THD v using evolutionary programming," Turkish Journal of Electrical Engineering & Computer Sciences, vol. 21, pp. 2269–2282, 2013, doi: 10.3906/elk-1205-35.

[33] D. Zhang, Z. Fu, and L. Zhang, "An improved TS algorithm for loss-minimum reconfiguration in large-scale distribution systems," Electric Power Systems Research, vol. 77, no. 5–6, pp. 685–694, Apr. 2007, doi: 10.1016/j.epsr.2006.06.005.

[34] H. H. Youssef, H. Mokhlis, M. S. A. Talip, M. A. Samman, M. A. Muhammad, and N. N. Mansor, "Distribution network reconfiguration based on artificial network reconfiguration for variable load profile," Turkish Journal of Electrical Engineering & Computer Sciences, vol. 28, no. 5, pp. 3013–3035, Sep. 2020, doi: 10.3906/elk-1912-89.

APPENDICES

Appendix A IEEE 33 Line Data

Branch number	Sending end bus	Receiving end bus
1	1	2
2	2	3
3	3	4
4	4	5
5	5	6
6	6	7
7	7	8
8	8	9
9	9	10
10	10	11
11	11	12
12	12	13
13	13	14
14	14	15
15	15	16
16	16	17
17	17	18
18	2	19
19	19	20
20	20	21
21	21	22
22	3	23
23	23	24
24	24	25
25	6	26
26	26	27
27	27	28
28	28	29
29	29	30
30	30	31
31	31	32
32	32	33

Appendix B IEEE 33 Bus Data

Bus number	P (kW)	Q (kVAR)
1	0	0
2	100	60
3	90	40
4	120	80
5	60	30
6	60	20
7	200	100
8	200	100
9	60	20
10	60	20
11	45	30
12	60	35
13	60	35
14	120	80
15	60	10
16	60	20
17	60	20
18	90	40
19	90	40
20	90	40
21	90	40
22	90	40
23	90	50
24	420	200
25	420	200
26	60	25
27	60	25

Appendix B (continued)

28	60	20
29	120	70
30	200	600
31	150	70
32	210	100
33	60	40

Appendix C IEEE 69 Line Data

Branch number	Sending end bus	Receiving end bus
1	1	2
2	2	3
3	3	4
4	4	5
5	5	6
6	6	7
7	7	8
8	8	9
9	9	10
10	10	11
11	11	12
12	12	13
13	13	14
14	14	15
15	15	16
16	16	17
17	17	18
18	18	19
19	19	20
20	20	21
21	21	22
22	22	23
23	23	24
24	24	25
25	25	26
26	26	27
27	3	28
28	28	29
29	29	30
30	30	31
31	31	32
32	32	33
33	33	34
34	34	35
35	3	36
36	36	37
37	37	38
38	38	39
39	39	40
40	40	41
41	41	42
42	42	43
43	43	44
44	44	45
45	45	46
46	4	47
47	47	48
48	48	49
49	49	50
50	8	51
51	51	52
52	9	53
53	53	54
54	54	55
55	55	56
56	56	57

Appendix C (continued)

57	57	58
58	58	59
59	59	60
60	60	61
61	61	62
62	62	63
63	63	64
64	64	65
65	11	66
66	66	67
67	12	68
68	68	69

Appendix D IEEE 69 Bus Data

Bus number	P (kW)	Q (kVAR)
6	2.6	2.2
7	40.4	30
8	75	54
9	30	22
10	28	19
11	145	104
12	145	104
13	8	5
14	8	5.5
16	45.5	30
17	60	35
18	60	35
20	1	0.6
21	114	81
22	5	3.5
24	28	20
26	14	10
27	14	10
28	26	18.6
29	26	18.6
33	14	10
34	19.5	14
35	6	4
36	26	18.55
37	26	18.55
39	24	17
40	24	17
41	1.2	1
43	6	4.3
45	39.22	26.3
46	39.22	26.3
48	79	56.4
49	384.7	274.5
50	384.7	274.5
51	40.5	28.3
52	3.6	2.7
53	4.35	3.5
54	26.4	19
55	24	17.2
59	100	72
61	1244	888
62	32	23
64	227	162
65	59	42
66	18	13
67	18	13
68	28	20
69	28	20

Appendix E IEEE 118 Line Data

Branch number	Sending end bus	Receiving end bus
1	0	1
2	1	2
3	2	3
4	2	4
5	4	5
6	5	6
7	6	7
8	7	8
9	8	9
10	2	10
11	10	11
12	11	12
13	12	13
14	13	14
15	14	15
16	15	16
17	16	17
18	11	18
19	18	19
20	19	20
21	20	21
22	21	22
23	22	23
24	23	24
25	24	25
26	25	26
27	26	27
28	4	28
29	28	29
30	29	30
31	30	31
32	31	32
33	32	33
34	33	34
35	34	35
36	30	36
37	36	37
38	29	38
39	38	39
40	39	40
41	40	41
42	41	42
43	42	43
44	43	44
45	44	45
46	45	46
47	35	47
48	47	48
49	48	49
50	49	50
51	50	51
52	51	52
53	52	53
54	53	54
55	28	55
56	55	56
57	56	57
58	57	58
59	58	59
60	59	60
61	60	61
62	61	62
63	1	63
64	63	64
65	64	65

Appendix E (continued)

66	65	66
67	66	67
68	67	68
69	68	69
70	69	70
71	70	71
72	71	72
73	72	73
74	73	74
75	74	75
76	75	76
77	76	77
78	64	78
79	78	79
80	79	80
81	80	81
82	81	82
83	82	83
84	83	84
85	84	85
86	79	86
87	86	87
88	87	88
89	65	89
90	89	90
91	90	91
92	91	92
93	92	93
94	93	94
95	94	95
96	91	96
97	96	97
98	97	98
99	98	99
100	1	100
101	100	101
102	101	102
103	102	103
104	103	104
105	104	105
106	105	106
107	106	107
108	107	108
109	108	109
110	109	110
111	110	111
112	111	112
113	112	113
114	100	114
115	114	115
116	115	116
117	116	117
118	117	118

Appendix F IEEE 118 Bus Data

Bus number	P (kW)	Q (kVAR)
1	0	0
2	133.84	101.14
3	16.214	11.292
4	34.315	21.845
5	73.016	63.602
6	144.2	68.604
7	104.47	61.725
8	28.547	11.503
9	87.56	51.073

Appendix F (continued)

10	198.2	106.77
11	146.8	75.995
12	26.04	18.687
13	52.1	23.22
14	141.9	117.5
15	21.87	28.79
16	33.37	26.45
17	32.43	25.23
18	20.234	11.906
19	156.94	78.523
20	546.29	351.4
21	180.31	164.2
22	93.167	54.594
23	85.18	39.65
24	168.1	95.178
25	125.11	150.22
26	16.03	24.62
27	26.03	24.62
28	594.56	522.62
29	120.62	59.117
30	102.38	99.554
31	513.4	318.5
32	475.25	456.14
33	151.43	136.79
34	205.38	83.302
35	131.6	93.082
36	448.4	369.79
37	440.52	321.64
38	112.54	55.134
39	53.963	38.998
40	393.05	342.6
41	326.74	278.56
42	536.26	240.24
43	76.247	66.562
44	53.52	39.76
45	40.328	31.964
46	39.653	20.758
47	66.195	42.361
48	73.904	51.653
49	114.77	57.965
50	918.37	1205.1
51	210.3	146.66
52	66.68	56.608
53	42.207	40.184
54	433.74	283.41
55	62.1	26.86
56	92.46	88.38
57	85.188	55.436
58	345.3	332.4
59	22.5	16.83
60	80.551	49.156
61	95.86	90.758
62	62.92	47.7
63	478.8	463.74
64	120.94	52.006
65	139.11	100.34
66	391.78	193.5
67	27.741	26.713
68	52.814	25.257
69	66.89	38.713
70	467.5	395.14
71	594.85	239.74
72	132.5	84.363
73	52.699	22.482
74	869.79	614.775
75	31.349	29.817

Appendix F (continued)

76	192.39	122.43
77	65.75	45.37
78	238.15	223.22
79	294.55	162.47
80	485.57	437.92
81	243.53	183.03
82	243.53	183.03
83	134.25	119.29
84	22.71	27.96
85	49.513	26.515
86	383.78	257.16
87	49.64	20.6
88	22.473	11.806
89	62.93	42.96
90	30.67	34.93
91	62.53	66.79
92	114.57	81.748
93	81.292	66.526
94	31.733	15.96
95	33.32	60.48
96	531.28	224.85
97	507.03	367.42
98	26.39	11.7
99	45.99	30.392
100	100.66	47.572
101	456.48	350.3
102	522.56	449.29
103	408.43	168.46
104	141.48	134.25
105	104.43	66.024
106	96.793	83.647
107	493.92	419.34
108	225.38	135.88
109	509.21	387.21
110	188.5	173.46
111	918.03	898.55
112	305.08	215.37
113	54.38	40.97
114	211.14	192.9
115	67.009	53.336
116	162.07	90.321
117	48.785	29.156
118	33.9	18.98